

# PCCP

Accepted Manuscript



This is an *Accepted Manuscript*, which has been through the Royal Society of Chemistry peer review process and has been accepted for publication.

*Accepted Manuscripts* are published online shortly after acceptance, before technical editing, formatting and proof reading. Using this free service, authors can make their results available to the community, in citable form, before we publish the edited article. We will replace this *Accepted Manuscript* with the edited and formatted *Advance Article* as soon as it is available.

You can find more information about *Accepted Manuscripts* in the [Information for Authors](#).

Please note that technical editing may introduce minor changes to the text and/or graphics, which may alter content. The journal's standard [Terms & Conditions](#) and the [Ethical guidelines](#) still apply. In no event shall the Royal Society of Chemistry be held responsible for any errors or omissions in this *Accepted Manuscript* or any consequences arising from the use of any information it contains.

## ARTICLE

## Luminescence studies in SnO<sub>2</sub> and SnO<sub>2</sub>:Eu nanocrystals grown by laser assisted flow deposition

Cite this: DOI: 10.1039/x0xx00000x

N. F. Santos<sup>a</sup>, J. Rodrigues<sup>a</sup>, T. Holz<sup>a</sup>, N. Ben Sedrine<sup>a</sup>, A. Sena<sup>a</sup>, A. J. Neves<sup>a</sup>, F. M. Costa<sup>a</sup>, T. Monteiro<sup>a</sup>Received 00th January 2012,  
Accepted 00th January 2012

DOI: 10.1039/x0xx00000x

www.rsc.org/

Transparent conductive tin oxide materials have been a research topic extensively studied in recent years due to the great interest for many applications. However, in most of them, the pure form is rarely used, being usually modified by the incorporation of dopants. Selecting the most appropriate technique to develop nanocrystals of doped tin oxide and understanding the influence of dopant on the optical properties are challenges that need to be addressed when envisaging devices. To fulfill this objective, the recently developed laser assisted flow deposition (LAFD) method is explored to grow SnO<sub>2</sub> and SnO<sub>2</sub>:Eu nanocrystals. The morphology of these nanocrystals was investigated by scanning electron microscopy and well defined prismatic habits with sizes of ~60 nm were identified. The crystalline quality assessed by X-ray diffraction measurements and Raman spectroscopy indicates that the produced nanocrystals are monophasic and crystallize in the tetragonal rutile structure. Steady state luminescence studies provide the information on the optical active centres in the SnO<sub>2</sub> and SnO<sub>2</sub>:Eu nanocrystals. For the undoped samples only broad emission bands were observed by pumping the samples in the ultraviolet region. The broad emission was found to be an overlap of green and red optical centres as identified by temperature and excitation intensity dependent luminescence. The latter was found to have an excitonic-related behaviour and the green emission was found to be of utmost importance to discuss the intraionic luminescence in the doped samples. For the SnO<sub>2</sub>:Eu nanocrystals the luminescence is dominated by the magnetic allowed <sup>5</sup>D<sub>0</sub>→<sup>7</sup>F<sub>1</sub> transition with the ions in almost undistorted centrosymmetric sites. The ion luminescence integrated intensity is found to increase with increasing temperatures being well accounted for a thermal population provided by the thermal quenching of the green band.

### Introduction

Metal oxides such as SnO<sub>2</sub> are known to be relevant materials for electronic applications including transparent conductive oxides (TCOs), dye sensitized solar cells (DSSCs), oxidation catalyst, chemical sensors and functional coatings [1-6]. This intrinsic n-type semiconductor [1,2,7,8], with dipole forbidden direct bandgap energy of ~ 3.6 eV at room temperature [1,9, 10], crystallizes in the tetragonal rutile structure [1,11]. When intentionally doped with lanthanides the transparent oxide also exhibit as advantage the possibility to spread the energetic levels of the trivalent charged lanthanide ions, being suitable for the developing of lanthanide-based optical emitters. Several approaches have been used in the material processing either in the form of powders, thin films, and more recently in synthesized nanostructures [9,12,13]. Despite the well-established knowledge on the structural and electrical tin oxide properties [1], the identification of the material optically active defects have been studied in less extent either in undoped and

intentionally doped SnO<sub>2</sub>. Excitonic transitions and donor acceptor pair (DAP) recombination were reported by Blattner *et al.* [14] in single crystals. Moreover, unstructured broad luminescence bands were also observed in single crystals [14], thin films [15] and nanostructures [13,16,17] in a wide spectral range from green to red.

Recently, Rodrigues *et al.*, [18-21] developed a new technique, the laser assisted flow deposition (LAFD), where a high power infrared laser is focused on the top of a precursor rod promoting the material decomposition and recombination under a self-catalytic vapour-liquid-solid mechanism for the nucleation and growth. Due to the principle of the method, this technique is suitable to synthesize nanocrystals of materials having close melting and evaporation points, such as the case of ZnO [18-21] and SnO<sub>2</sub> [21]. The temperature gradient generated inside the growth chamber allows the material flux deposition on a substrate localized strategically above the region where the reaction occurs. Taking into account that the process occurs

inside a growth chamber, the synthesis atmosphere can be controlled, being a catalyst-free technique, easily scalable. In this work, the LAFD method was explored to synthesise undoped and europium-doped tin oxide nanostructures deposited on silicon substrates. The nanocrystals of SnO<sub>2</sub> and SnO<sub>2</sub>:Eu were morphologically and optically characterized. A detailed study of the temperature dependent PL measurements was also performed on both types of samples. Additionally, excitation intensity dependent photoluminescence (PL) studies, room temperature (RT) PL excitation (PLE) and time resolved PL (TRPL) measurements were carried out in order to establish the nature of a red broad band optical centre in the undoped samples. The excitation and de-excitation processes of the measured luminescence in the undoped and doped nanocrystals is analysed and discussed.

## Experimental details

The laser assisted flow deposition was performed on a modified laser floating zone (LFZ) growth chamber which comprises a 200 W CO<sub>2</sub> laser (Spectron) coupled to a reflective optical set-up producing a circular crown-shaped laser beam, as reported elsewhere [18-21]. The rods were prepared by mixing the initial SnO<sub>2</sub> powders with polyvinyl alcohol (PVA), obtaining a slurry that was further extruded into cylindrical rods with diameters of 1.75 mm. For the doped samples, a nominal 3.0 mol% of Eu<sub>2</sub>O<sub>3</sub> was used in the mixture. Figure 1 shows a picture of the growth apparatus. The beam was focused at the tip of the extruded rods and Si {001} substrates were placed on a sample holder attached to the upper spindle of the LFZ system, above the feed rod. The laser beam was focus on the tip of the precursor leading to the material evaporation. This method is favoured due to the proximity of the melting and ebullition temperatures together with the local heating generated by the high power laser focused on the top of the extruded rod. The generated gases are then transferred to the low temperature regions where the substrate is placed, after a recombination of tin with oxygen to form SnO<sub>2</sub> products. This process occurs in few minutes (~3 min) and the laser power was varied between 25 W to 35 W. A distance of 5 mm from the precursor to the substrate was kept constant as well as other parameters such as angular velocities of the substrate and precursors (5 rpm) and linear velocity of the precursor (100 mm.h<sup>-1</sup>). The growth process was performed in air at atmospheric pressure.

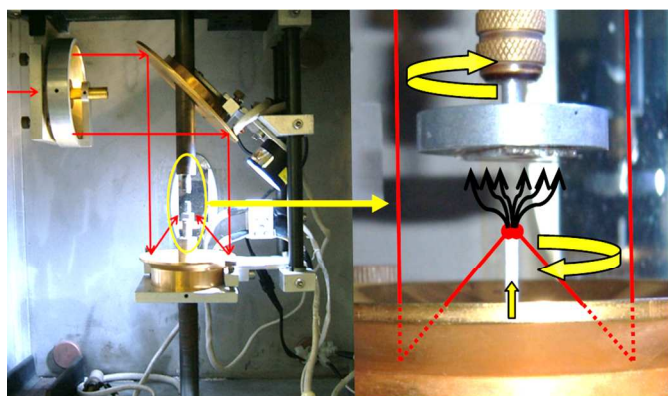


Figure 1 – LAFD growth apparatus.

The samples morphology and microstructure were characterized by SEM (Hitachi SU-70 system). Energy dispersive spectroscopy (EDS) measurements were performed in a TESCAN Vega3 SBH SEM equipped with a peltier-cooled Bruker XFlash 410-M silicon drift detector (energy resolution of 133 eV at Mn K<sub>α</sub>) and a Quantax microanalysis system. The crystalline structure of the nanocrystals was investigated by XRD using a PANalytical X'Pert PRO apparatus. Raman spectra were measured in backscattering configuration at room temperature (RT), by exciting the samples with the 442 nm line of a cw He-Cd laser by using a Horiba Jobin-Yvon HR800 set up. Steady state PL measurements were carried out between 14 K and the RT using the 325 nm He-Cd laser line as excitation source excitation with a power density less than 0.6 W.m<sup>-2</sup>. Additionally, the doped samples were excited with the 395 nm wavelength photons. The luminescence was measured using a dispersive system, a single grating SPEX 1704 monochromator (1 m, 1200 gr.mm<sup>-1</sup>), fitted with a cooled Hamamatsu R928 photomultiplier tube.

The RT PLE was assessed in a Fluorolog-3 Horiba Scientific modular equipment with a double additive grating Gemini 180 scanning monochromator (2×180 mm, 1200 gr.mm<sup>-1</sup>) in the excitation and a triple grating iHR550 spectrometer in the emission (550 mm, 1200 gr.mm<sup>-1</sup>). A 450 W Xe lamp was used as excitation source. The PLE was assessed by setting the emission monochromator in the maxima of the optically active defects and the excitation was scanned to higher energies. The measurements were performed using a front face acquisition mode, and were corrected to the optical components and to the Xe lamp spectral responses. RT time resolved (TRPL) spectra were acquired with the same Fluorolog-3 system using a pulsed Xe lamp coupled to a monochromator.

## Results and discussion

### Structural and morphological analysis

Figure 2 shows typical XRD diffraction patterns of the LAFD produced SnO<sub>2</sub> and SnO<sub>2</sub>:Eu nanocrystals. The set of the diffraction maxima matches well those expected for the SnO<sub>2</sub> tetragonal rutile structure (cassiterite), in line with the indexation of the standard data file JCPDS (21-1250).

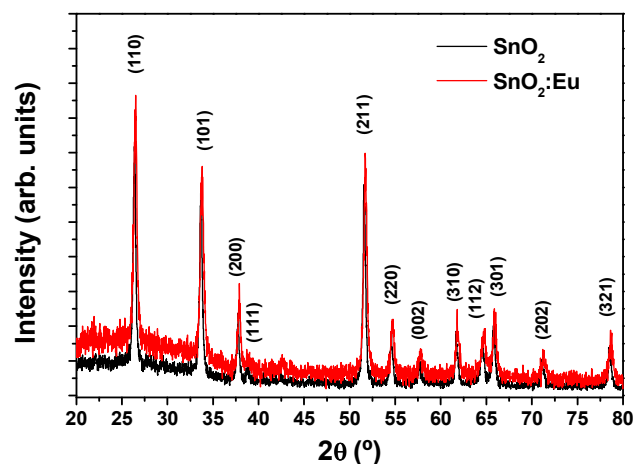
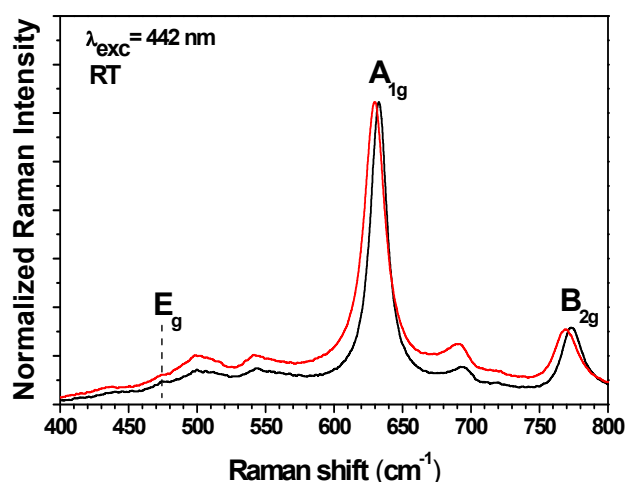


Figure 2 – XRD diffraction patterns of the undoped (black line) and Eu doped (red line) LAFD SnO<sub>2</sub> nanocrystals grown at 35 W and 25 W, respectively.

No additional crystalline phases were identified in the nominally undoped and europium doped samples, indicating that high crystalline quality monophasic nanocrystals are promoted under the used LAFD growth parameters. It should be emphasized that the absence of secondary phases is in contrast with previous reported results for doped samples by a distinct approach [22] where the addition of  $\text{Eu}_2\text{O}_3$  contents higher than 0.01 mol. % lead to the appearance of additional diffraction maxima. From the obtained diffractograms the lattice parameters of the tetragonal lattice were estimated and the values of  $a = 4.75 \text{ \AA}$  and  $c = 3.19 \text{ \AA}$  were determined for the undoped tin oxide. In the case of the  $\text{SnO}_2:\text{Eu}$  nanocrystals values of  $a = 4.73 \text{ \AA}$  and  $c = 3.18 \text{ \AA}$  were obtained. In both cases, the data are similar to those reported in the literature for tin oxide [1, 23] but a direct comparison between the lattice parameters of the undoped and doped samples suggests a slight contraction of the lattice in the presence of the europium dopant.



**Figure 3** – Normalized Raman spectra of the undoped (black line) and Eu doped (red line) LAFD  $\text{SnO}_2$  nanocrystals grown at 30 W and 25 W, respectively. The spectra were obtained with the 442 nm laser line in backscattering configuration.

Similarly to the XRD, Raman spectroscopy revealed the same signature for all samples regardless the laser power used in the synthesis process and the presence of dopant. The identification of the tetragonal rutile crystalline phase was corroborated by the Raman spectra. Typical spectra of the produced samples are shown in Figure 3. With two molecules per unit cell, eighteen normal vibrational modes are expected near the  $\Gamma$  ( $\vec{q} \approx 0$ ) point of the first Brillouin zone for the material crystallizing in the tetragonal rutile structure (point group  $D_{4h}^{14}$ ). As in the case of the single crystals [1,24-26], three of the four active Raman modes having  $E_g$ ,  $A_{1g}$  and  $B_{2g}$  symmetries were identified in the high frequency range at  $475 \text{ cm}^{-1}$ ,  $633 \text{ cm}^{-1}$  and  $774 \text{ cm}^{-1}$ , respectively. Additionally, a full width at half maximum broadening of  $\sim 4 \text{ cm}^{-1}$  as well as a  $\sim 3 \text{ cm}^{-1}$  redshift of the vibrational modes were observed in the doped sample, likely due to lattice distortions. Disorder activated resonances ( $\vec{q} \neq 0$ ), depending on the particle size and samples' synthesis temperature, were also observed in the  $475$  to  $775 \text{ cm}^{-1}$  region as reported by others [25].

The crystals morphology assessed by SEM is displayed in Figure 4. From the inspection of the SEM micrograph is possible to infer that the applied laser power only affects the amount of deposited material during the growth. Independently of the used power during the growth process, the morphology of the  $\text{SnO}_2$  and  $\text{SnO}_2:\text{Eu}$  nanocrystals is always polyhedral exhibiting bipyramidal structures which constitute typical habits of the tin oxide material [27,28]. These crystals have a uniform sizes distribution of  $\sim 60 \text{ nm}$ . EDS measurements revealed that the amount of Eu present in the sample is below the detection limit of the EDS system (0.1 mol %) hampering the doping quantification. It was found that most of the Eu content remains in the precursors and does not evaporate. This is not a surprising result since it is known from previous reports that the solubility of the Eu ions in this matrix is low (around 0.05 mol. % [29]). Moreover, since the LAFD depends on the proximity of the melting and ebullition temperatures it is not expected the production of other Eu compounds, like  $\text{Eu}_2\text{O}_3$ , due to the significant difference between these two quantities for this material.

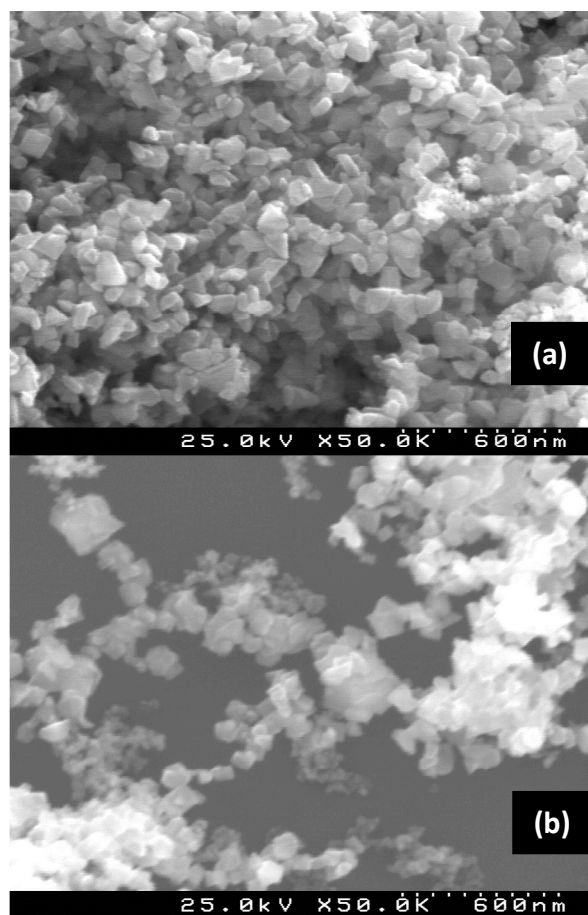


**Figure 4** – Scanning electron microscopy images of  $\text{SnO}_2$  nanostructures grown by LAFD: (a)  $\text{SnO}_2$  growth at 30 W laser power; (b)  $\text{SnO}_2:\text{Eu}$  growth at 25 W laser power.

### Luminescence studies

**SnO<sub>2</sub> nanocrystals.** Despite the interest of the material for several electronic and sensor applications, the exploitation of the optically active defects in tin oxide deserves an in-depth investigation. Figure 5 shows the temperature dependent PL of the LAFD SnO<sub>2</sub> nanocrystals synthesized using 30 W laser power.

By exciting the SnO<sub>2</sub> nanostructures in the absorption edge with 3.8 eV (325 nm) energy photons, the luminescence of the undoped samples at 14 K is dominated by a broad unstructured emission band extending from the ultraviolet to the near infrared due to overlapped emitting centres.

The temperature dependent PL spectra reveal that the shoulder in the green spectral region (on the higher energy side of the broad band) suffers a strong luminescence thermal quenching between 14 K and 150 K. For higher temperatures, the PL spectra are peaked on the red region ~660 nm (1.88 eV) and no additional changes on the spectral shape and peak position occur up to RT. As aforementioned, such PL behaviour is typical of overlapped optical emitting centres with distinct de-excitation pathways. In order to further investigate the two optical centres (green and red emission bands) by using a deconvolution of the overall luminescence, excitation intensity dependent PL studies were realized at RT.

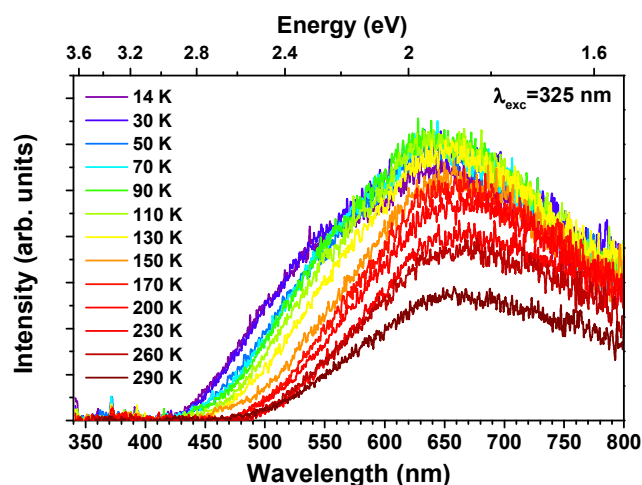


**Figure 5** – Temperature dependent PL spectra of the LAFD SnO<sub>2</sub> nanocrystals synthesized with 30 W of laser power. The spectra were obtained with 3.8 eV photon excitation.

Figure 6a depicts the PL spectra at RT obtained under different excitation powers, while Figure 6b shows a log(I/I<sub>0</sub>)-log(P/P<sub>0</sub>) plot of the above mentioned emission, where *I* corresponds to the integrated intensity and *P* is the excitation power. By decreasing the excitation intensity over one decade no changes on the spectral shape and peak position were identified. These results, together with the slope obtained for the power law,  $I \sim P^k$ , suggest that a mechanism involving DAP transitions could be discarded as a recombination model for the red PL band. Excitation power dependence of the red integrated PL was well accounted by a power law with a unitary slope *k* in a log-log plot. According to Schmidt *et al.* [30], a unitary slope suggests an exciton-like transition involving a deep level defect. Therefore, and at low temperatures, the experimental data are consistent with one optical centre peaked at ~660 nm (1.88 eV) which is responsible of the red luminescence,

overlapped with a high energy emission band which accounts for the shoulder observed in the green spectral region as shown in Figure 5.

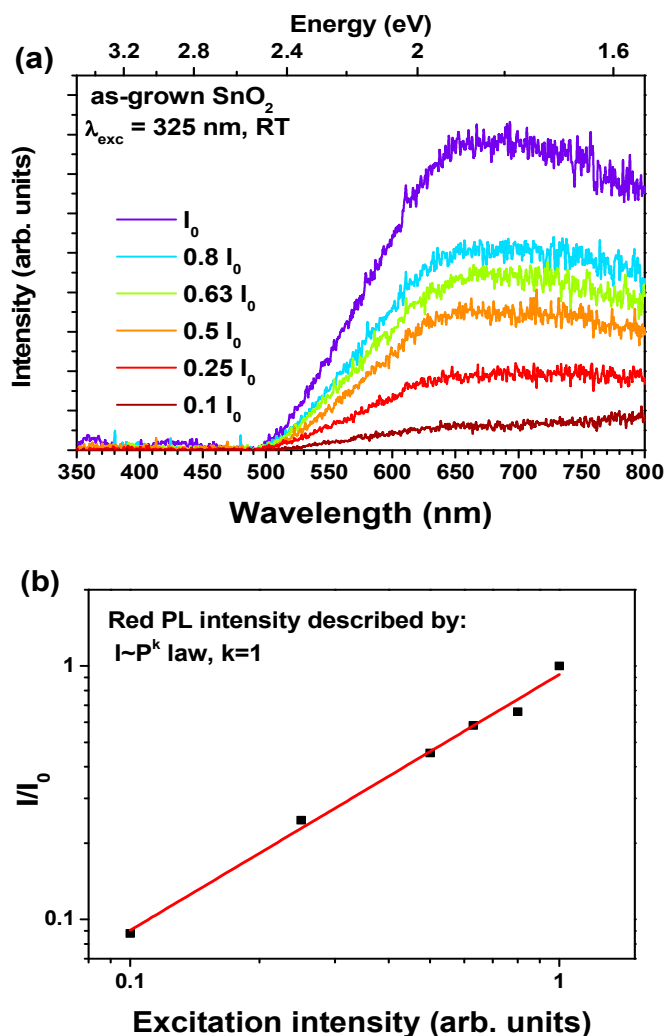


**Figure 6** – a) RT excitation intensity dependent red PL spectra for the LAFD SnO<sub>2</sub> nanocrystals synthesized with 30 W of laser power obtained with 325 nm photon excitation. The reduction of the excitation intensity was obtained by using several neutral density filters. b) Dependence of the red band integrated intensity as a function of the excitation intensity. Full line corresponds to the best fit of the experimental data.

The temperature dependent PL spectra were deconvoluted by two Gaussian shaped PL bands with maxima at ~514 nm (2.4 eV) and ~660 nm (1.88 eV) and full widths at half maximum of 440 meV and 575 meV at 14 K, respectively (Figure 7a). Broad emission bands from the violet to infrared have been reported in SnO<sub>2</sub> single crystals, thin films, sintered polycrystalline materials and nanocrystals [14-16,22,31-40]. However, the chemical nature of the defects that originate such large visible bands is still a matter of debate in the literature, being the intrinsic defects, like the oxygen vacancies and unwanted impurities, currently pointed out as the main sources for the broad PL bands [14-16,22,31-40].

Figure 7b) shows the temperature dependent integrated PL intensity for the green and red bands obtained from the

Gaussian fits to the two emitting centres between 14 K and 110 K. For higher temperatures only the red luminescence prevails. A strong thermal quenching of the green PL band is clearly seen, being the emission almost absent for temperatures above 100 K. Under the assumption that the nonradiative deactivation processes can be treated classically by a Mott law, the temperature dependence of the integrated intensity of the green and red bands is well described by the  $I(T) = I_0 \cdot [1 + C \exp(-E_a/k_B T)]^{-1}$  equation, where  $E_a$  stands for the activation energy of the nonradiative processes,  $k_B$  the Boltzmann constant,  $I_0$  the integrated intensity at low temperature and  $C$  a pre-exponential factor which accounts for the energy levels degeneracy.

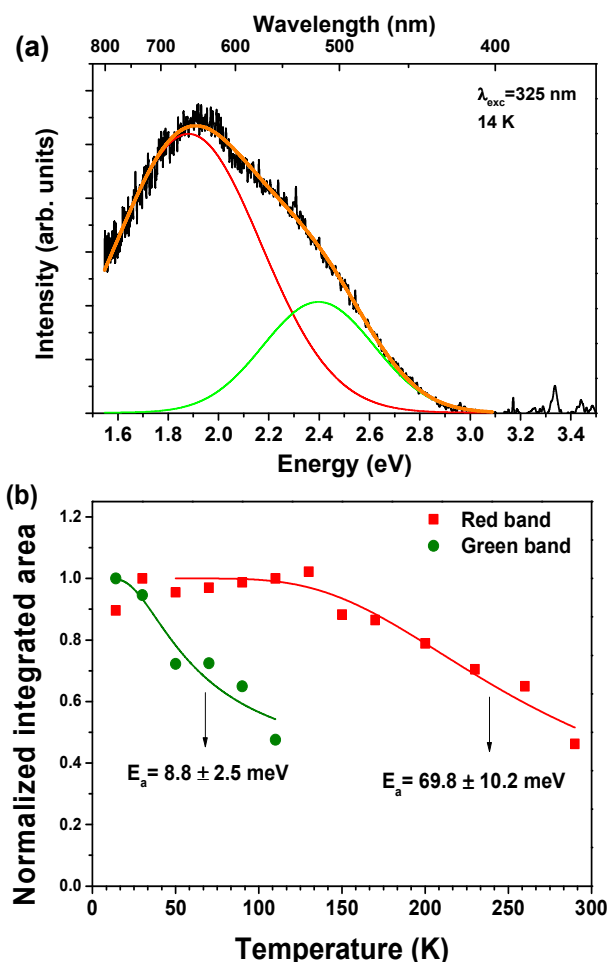


**Figure 7** – a) 14 K PL spectrum and deconvolution by two Gaussian shaped broad bands peaked at 2.4 eV (516 nm) and 1.88 eV (660 nm). The luminescence was excited with 325 nm wavelength photons. b) Temperature dependent integrated intensity for the green and red PL bands.

The best fits to the experimental data shown in Figure 7b) correspond to activation energies of  $8.8 \pm 2.5$  meV and  $69.8 \pm 10.2$  meV with pre-exponential factors of  $2.2 \pm 0.9$  and  $15.3 \pm 7.7$  for the green ( $\sim 2.4$  eV) and red ( $\sim 1.88$  eV) bands, respectively. The fast quenching of the high energy band shows a similar tendency to those earlier reported in  $\text{SnO}_2$  samples processed/ synthesized by different routes [14-16, 22, 31-40]. However, the peak position of the reported PL bands depends on the growth method and/or growth parameters used [14-16, 22, 31-40]. Moreover, Maestre *et al.* [37, 39] show by RT

panchromatic cathodoluminescence that the green, yellow and red PL broad bands in  $\text{SnO}_2$  are strongly correlated with the defects distribution in the distinct crystallite facets of the microcrystals and grain boundaries in sintered polycrystalline material. Contrarily to the green band, the red emission shows a higher stability at low temperatures as identified by the constancy of the integrated PL. For this optical centre, the non-radiative processes which compete with the radiative ones start to be meaningful for temperatures above 150 K.

**$\text{SnO}_2$ :Eu nanocrystals.** The behaviour of the luminescence investigated in the  $\text{SnO}_2$  nanocrystals processed by LAFD was found to be of utmost importance for the exploitation of PL in the  $\text{SnO}_2$ :Eu nanocrystals. As shown in Figure 8, the intra- $4f^6$  lines of  $\text{Eu}^{3+}$  ions were observed for the *in-situ* doped nanostructures. Independently of the growth conditions, the emission from the  $\text{SnO}_2$ :Eu nanocrystals is dominated by the orange/red ions luminescence composed by atomic-like lines as expected for the ions placed in well-defined crystalline environment. These lines appear overlapped with the broad band observed in the undoped samples (Figure 8a). The  $\text{Eu}^{3+}$  emission is mainly due to the  $^5\text{D}_0 \rightarrow ^7\text{F}_{0,2}$  transitions. The forbidden  $^5\text{D}_0 \rightarrow ^7\text{F}_0$  line occurs at 584 nm and the emission among the  $^5\text{D}_0$  and  $^7\text{F}_1$  manifolds exhibit a full  $2J+1$  lifted degeneracy with the three lines peaked at 587.5 nm, 592.7 nm and 598.7 nm. This magnetic allowed transition corresponds to the  $\text{Eu}^{3+}$  emission with the highest intensity. Minor intensity lines assigned to the hypersensitive  $^5\text{D}_0 \rightarrow ^7\text{F}_2$  transition are observed at 609 nm and 611 nm. Similar spectra were reported earlier for europium doped  $\text{SnO}_2$  single crystals [41] and polycrystalline samples produced by sol-gel [42,43], combustion synthesis [44], solvothermal [45] and sinterization [22]. The observation of the  $^5\text{D}_0 \rightarrow ^7\text{F}_0$  transition together with the analysis of the relative intensity between the forced dipole electric  $^5\text{D}_0 \rightarrow ^7\text{F}_2$  and the magnetic dipole allowed  $^5\text{D}_0 \rightarrow ^7\text{F}_1$  lines (asymmetric ratio  $^5\text{D}_0 \rightarrow ^7\text{F}_2 / ^5\text{D}_0 \rightarrow ^7\text{F}_1$ ) are usually used to explore the number of  $\text{Eu}^{3+}$  optically active sites in a given lattice [46,47]. In particular, due to the non-degenerate character of the  $^7\text{F}_0$  fundamental and  $^5\text{D}_0$  excited levels, the number of observed lines resulting from transitions between the  $^5\text{D}_0 \rightarrow ^7\text{F}_0$  multiplets gives an indication of the number of  $\text{Eu}^{3+}$  environments [46,47]. In the LAFD processed  $\text{SnO}_2$ :Eu nanocrystals the observation of a single narrower  $^5\text{D}_0 \rightarrow ^7\text{F}_0$  line suggests an europium dominant environment in the  $\text{SnO}_2$  lattice. Furthermore, lanthanides are known to preferentially substitute the cations in a given matrix and as pointed by others [41-43] it is likely to assume that in  $\text{SnO}_2$  crystal  $\text{Eu}^{3+}$  substitute  $\text{Sn}^{4+}$  in sites were further charge compensation occurs. Therefore  $\text{Eu}^{3+}$  ions in our samples should be placed in almost undistorted centrosymmetric sites accordingly with previous investigations [41-43]. Figure 8a) also depicts the PLE spectrum monitored in the most intense line of the  $\text{Eu}^{3+}$   $^5\text{D}_0 \rightarrow ^7\text{F}_1$  transition and on the maximum of the broad red band. Both optical centres are preferentially populated by a broad UV excitation band with an onset absorption at 450 nm and with the maximum extending into the  $\text{SnO}_2$  band gap. The data clear indicate that an efficient energy transfer from the host to the Eu ions occur via the above band gap excitation as expected for the ions substituting the  $\text{Sn}^{4+}$  sites. Nevertheless, different contribution for the UV band may appear overlapped in this spectral region, namely the band edge of the semiconductor host, an energy transfer band and the intraionic excited levels of the  $\text{Eu}^{3+}$  ion. Energy dependence studies were also performed by exciting with energies close to the expected the free-ion

europium excited states such those corresponding to the usual strong  ${}^7F_0 \rightarrow {}^5L_6$  absorption at 395 nm. Under this wavelength photon excitation no  $\text{Eu}^{3+}$  optical activation was identified indicating that secondary or amorphous phases containing optically active europium ions are missing in our samples, corroborating the absence of additional  $\text{Eu}^{3+}$  lines due to ions in low symmetry sites as observed by others [43]. RT TRPL spectra are shown in Figure 8b. The TRPL spectra obtained under different delays with a fixed time window of 0.2 ms show that the broad red band has similar spectral shape and peak position as the one measured with steady state conditions. The absence of low energy shifts in the band maxima with increasing delay times also corroborates the aforementioned excitonic model for the red band, namely as no DAP behaviour is identified with increasing delay times. On the other hand, the intensity of the broad red PL was found to suffer a fast decrease with increasing delay times meaning that the emission has a decay time in the range of hundreds of microseconds. On the contrary, the TRPL spectra evidence that the  ${}^5D_0 \rightarrow {}^7F_1$  transition of the  $\text{Eu}^{3+}$  ions have a longer lifetime in the range of few ms as identified by the well-resolved intra-ionic emission for higher delay times. Such long decay well matches the character of a magnetic allowed transition.

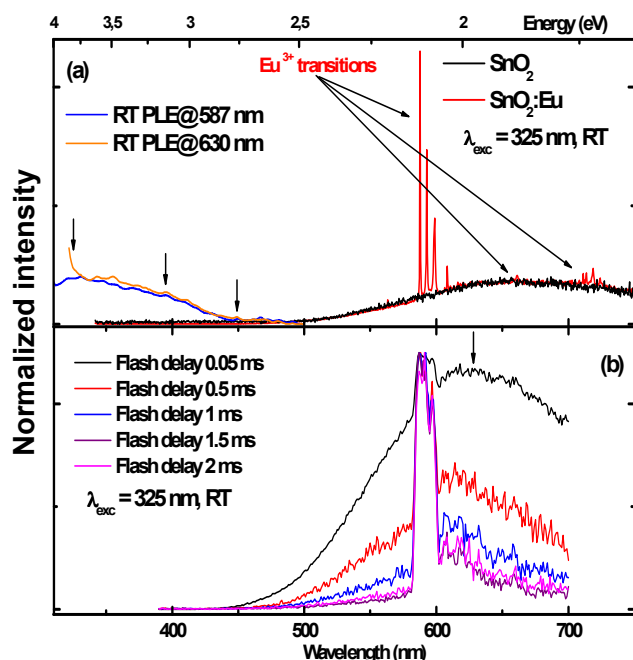


Figure 8 – a) RT PL/PLE spectra: comparison between the  $\text{SnO}_2$  and  $\text{SnO}_2:\text{Eu}$ . The arrows indicate the wavelengths where the doped sample was excited. b) Time-resolved PL spectra for the  $\text{SnO}_2:\text{Eu}$  nanocrystals with 4 different time delays and a fixed time window of 0.2 ms.

In order to get insights into the  $\text{Eu}^{3+}$  recombination processes, temperature dependent PL was carried out by pumping the sample with 325 nm photons as shown in Figure 9a). As identified, the temperature dependence of the  $\text{Eu}^{3+}$  integrated intensity (Figure 9b) reveals an opposite trend to the optical centres identified in the undoped nanocrystals. In fact, an increase of the integrated intensity was observed almost in the overall studied temperature range. Similar tendencies were also identified in xerogels where the decrease of the intensity for samples doped with 0.1 at. % and 0.5 at. % was found to occur

at 250 K and 200 K [43], respectively, suggesting that the decrease of the intensity at higher temperatures could be related with the ion content in the host. The increase in intensity is well accounted for a thermal assisted population of the emitting centre. As the europium transitions are overlapped with the same optical active defects of the undoped samples (Figure 8a), a likely candidate for the thermal population of  $\text{Eu}^{3+}$  ions corresponds to the green-related defect which shows faster thermal quenching. In fact, the solid line in Figure 9b) shows the best fit to a thermal population assuming a Boltzmann function with an activation energy of  $8.3 \pm 2.4$  meV and pre-exponential factor of  $2.3 \pm 0.6$ , suggesting that a correlation between the de-excitation processes of the green band and the  $\text{Eu}^{3+}$  increasing intensity could occur.

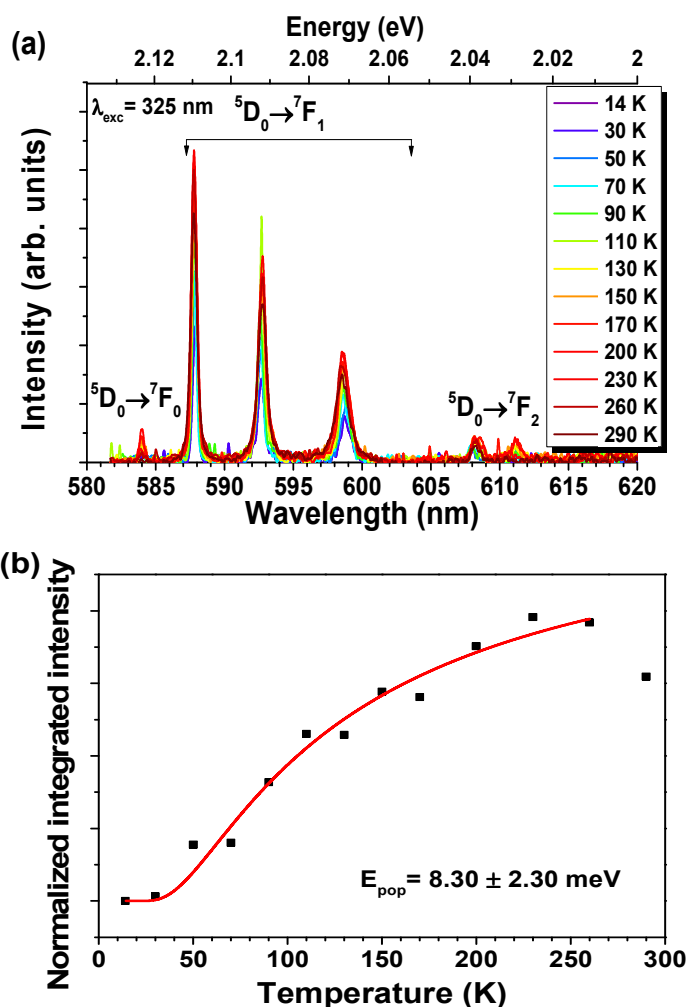


Figure 9 – a) Temperature dependent PL spectra for the  $\text{SnO}_2:\text{Eu}$  nanocrystals. b) Temperature dependent integrated  $\text{Eu}^{3+}$  PL intensity. PL was obtained with the 325 nm He-Cd line as excitation source.

## Conclusions

In summary, we have successfully synthesized undoped and europium doped tin oxide nanocrystals by the LAFD method. The produced nanocrystals show a very uniform size distribution with sizes of ~60 nm exhibiting well defined prismatic morphologies and high crystalline quality as assessed by XRD and Raman spectroscopy. Moreover, the LAFD method proved to be effective in doping effect. In fact, despite the reduced synthesis time (3 min) the europium ion was incorporated in the tin oxide host and no secondary crystalline phases were developed. The absence of crucible in this technique enables the development of more pure materials since there is no reaction of oxides with the crucible material that is common in the conventional synthesis methods.

The PL of the SnO<sub>2</sub> and SnO<sub>2</sub>:Eu nanocrystals were studied and in the set of undoped SnO<sub>2</sub> samples only broad emission bands were observed by pumping the samples in the ultraviolet. The broad emission was found to be an overlap of green and red optical centres as identified by temperature and excitation intensity dependent PL. The green band suffers a strong thermal quenching in the used temperature interval range. The red luminescence persists up to RT and has an excitonic-related behaviour as confirmed by the excitation dependent PL and corroborated by RT TRPL. The luminescence in the SnO<sub>2</sub>:Eu samples is dominated by the magnetic allowed <sup>5</sup>D<sub>0</sub>→<sup>7</sup>F<sub>1</sub> transition with the ions in almost undistorted centrosymmetric sites agreeing well with previous reports using different growth approaches. No other europium lines associated with the ions in low site symmetries were found, meaning that even with a nominal 3 mol. % Eu<sub>2</sub>O<sub>3</sub> amount the Eu ion solubility limit was not reached in the LAFD doped nanocrystals, as proved by EDS. The ion luminescence integrated intensity is found to increase with increasing temperatures being well accounted for a thermal population provided by the thermal quenching of the green band.

## Acknowledgements

The authors acknowledge financial support from FCT: PTDC/CTM-NAN/2156/2012, RECI/FIS-NAN/0183/2012 (FCOMP-01-0124-FEDER-027494), CENTRO-07-ST24-FEDER-002032, CENTRO-07-ST24-FEDER-002030 and UID/CTM/50025/2013. J. Rodrigues and N. F. Santos thank to FCT for their PhD grants, SFRH/BD/76300/2011 and SFRH/BD/90017/2012. The authors want to thank to A.F. Martins for his help in the experiments.

## Notes and references

<sup>a</sup> Physics Department and I3N, University of Aveiro, 3810-193 Portugal

- [1] M. Batzill, U. Diebold, *Prog. in Surf. Sci.*, 79 (2005) 47.
- [2] T. Oyabu, *J. Appl. Phys.*, 53 (1982) 2785.
- [3] N. Amin, T. Isaka, A. Yamada, M. Konagai, *Sol. Energy Mater. Sol. Cells*, 67 (2001) 195.
- [4] T. J. Courtts, X. Liand, T. A. Cessert, *IEEE Elec. Dev. Lett.*, 26 (1990) 660.
- [5] J. S. Maudes, T. Rodriguez, *Thin Sol. Films*, 69, (1980) 183.
- [6] G. Martinelli, M. C. Carotta, *Sens. Actuators A*, 15-16, (1993) 363.
- [7] H. J. van Daal, *Sol. St. Commun.*, 6 (1968) 5.
- [8] C. G. Fonstad, R. H. Rediker, *J. Appl. Phys.*, 42 (1971) 2911.
- [9] R. Summitt, J. A. Marley, N. F. Borrelli, *J. Phys. Chem. Sol.*, 25, (1964) 1465.
- [10] V. T. Agekyan, *phys. stat. sol. (a)*, 43 (1977) 11.
- [11] I. M. Tiginyanu, O. Lupan, V. V. Ursaki, L. Chow, M. Enachi, *3.11 - Nanostructures of Metal Oxides*, in *Comprehensive Semiconductor Science and Technology*, P. Bhattacharya, R. Fornari, and H. Kamimura, Eds., ed. Amsterdam: Elsevier, 2011, pp. 396-479
- [12] S. Goldsmith, E. Çetinörgü, R. Boxman, *Thin Sol. Films*, 517 (2009) 5146.
- [13] G. Salviati, L. Lazzarini, M. Z. Zha, V. Grillo, E. Carlino, *phy. sta. sol. (a)*, 202 (2005) 2963.
- [14] G. Blattner, C. Klingshirn, R. Helbig, *Sol. St. Commun.*, 33 (1980) 341.
- [15] J. Jeong, S.-P. Choi, C. I. Chang, D. C. Shin, J. S. Park, B. T. Lee, Y.-J. Park, H.-J. Song, *Sol. St. Commun.*, 127 (2003) 595.
- [16] S. Sarmah, A. Kumar, *Indian J. Phys.*, 84 (2010) 1211.
- [17] D. A. Popescu, J.-M. Herrmann, A. Ensuque, F. Bozon-Verduraz, *Phys. Chem. Chem. Phys.*, 3 (2001) 2522.
- [18] J. Rodrigues, M. Peres, M. R. N. Soares, A. J. S. Fernandes, N. Ferreira, M. Ferro, A. J. Neves, T. Monteiro, F. M. Costa, *J. Nano Res.*, 1819 (2012)129.
- [19] J. Rodrigues, M. Soares, R. Carvalho, A. Fernandes, M. Correia, T. Monteiro, F. M. Costa, " *Thin Sol. Films*, 520 (2012) 4717.
- [20] J. Rodrigues, A. J. S. Fernandes, D. Mata, T. Holz, R. G. Carvalho, R. Fath Allah, T. Ben, D. Gonzalez, R. F. Silva, A. F. da Cunha, M. R. Correia, L. C. Alves, K. Lorenz, A. J. Neves, F. M. Costa, T. Monteiro, *Proc. SPIE 8987, Oxide-based Materials and Devices V*, (2014) 89871F.
- [21] M. R. Soares, J. Rodrigues, N. F. Santos, C. Nico, R. G. Carvalho, A. J. S. Fernandes, M. P. Graça, L. Rino, M. J. Soares, A. J. Neves, F. M. Costa, T. Monteiro, *Proc. SPIE 8626, Oxide-based Materials and Devices IV*, (2013) 862607.
- [22] S.-Sik Chang, M.S. Jo, *Ceram. Internat.*, 33 (2007) 511.
- [23] R. Casali, J. Lasave, M. Caravaca, S. Koval, C. Ponce, R. Migoni, *J. Phys.: Condens. Matter*, 25 (2013) 135404.
- [24] P. S. Peercy, B. Morosin, *Phys. Rev. B*, 7, (1973) 2779.
- [25] A. Diéguez, A. Romano-Rodríguez, A. Vilà, J. R. Morante, *J. Appl. Phys.*, 90 (2001) 1550.
- [26] S. H. Sun, G. W. Meng, G. X. Zhang, T. Gao, B. Y. Geng, L. D. Zhang, J. Zuo, *Chem. Phys. Lett.*, 376 (2003) 103.
- [27] N. S. Ramgir, I. S. Mulla, K. P. Vijayamohan, *J. Phys. Chem. B*, 108 (2004) 14815.
- [28] H. W. Kim, S. H. Shim, C. Lee, *Ceram. Internat.*, 32 (2006) 943.
- [29] A. C. Yanes, J. Del Castillo, M. Torres, J. Peraza, V. D. Rodríguez, J. Méndez-Ramos, *Appl. Phys. Lett.*, 85 (2004) 2343.
- [30] T. Schmidt, K. Lischka, W. Zulehner, *Physical Review B*, 45 (1992) 8989.
- [31] E. Mollwo, D. Zwingel, *J. Lum.*, 12/13 (1976) 441.
- [32] N. Chiodini, A. Paleari, D. DiMartino, G. Spinolo, *Appl. Phys. Lett.*, 81 (2002) 1702.
- [33] E. Viana, J. González, G. Ribeiro, A. De Oliveira, *J. Phys. Chem. C*, 117 (2013) 7844.
- [34] J. P. Fillard, J. Gasiot, M. De Murcia, T. T. Quynh, *phys. Stat. sol. (a)*, 9 (1972) K169.

- [35] L. Suhua, F. Jiyang, L. Weili, Z. Miao, S. Zhitang, L. Chenglu, W. Xinglong, K. C. Paul, *Nanotech.*, 17, (2006) 1695.
- [36] S-Sik Changa, S.O. Yoon, H. Jeong Park, *Ceram. Internat.*, 31 (2005) 405.
- [37] S. Luo, J. Fan, W. Liu, M. Zhang, Z. Song, C. Lin, X. Wu, P. K. Chu, *Nanotech.*, 17 (2006) 1695.
- [38] D. Maestre, A. Cremades, J. Piqueras, *J. Appl. Phys.*, 95 (2004) 3027.
- [39] D. Maestre, A. Cremades, J. Piqueras, *J. Appl. Phys.*, 97 (2005) 044316.
- [40] H. T. Chen, X. L. Wu., S. J. Xiong, W. C. Zhang, J. Zhu, *Appl Phys A*, 97 (2009) 365.
- [41] D. F. Crabtree, *J. Phys. D: Appl. Phys.*, 8 (1975) 107.
- [42] G. E. S. Brito, S. J. L. Ribeiro, V. Briois, J. Dexpert-Ghys, C. V. Santilli, S. H. Pulcinelli, *J. Sol-Gel Sci. Techn.*, 8 (1997) 261.
- [43] E. A. Morais, L. V. A. Scalvi, A. Tabata, J. B. B. De Oliveira, S. J. L. Ribeiro, *J. Mater. Sci.*, 43 (2008) 345.
- [44] J. Hyuk Kang, J. Young Kim, D. Young Jeon, *J. Electrochem. Soc.*, 152, (2005) H33 (2005).
- [45] T. Moon, S.-T. Hwang, D.-R. Jung, D. Son, C. Kim, J. Kim, M. Kang, B. Park, *J. Phys. Chem. C*, 111 (2007) 4164.
- [46] G. Blasse, *Handbook on the Physics and Chemistry of Rare Earths*, Elsevier Science, North- Holland Physics Publishing, 1979, Vol. 4, p. 34.
- [47] G. Blasse and B. C. Grabmaier, *Luminescent Materials*, Springer, Berlin, 1994.